Preparation and Characterization of Carbon Nano-onions by Nanodiamond Annealing and Functionalization by Radio-frequency Ar/O_2 Plasma

Joanne P. Bartolome, Alex Fragoso*

Nanobiotechnology & Bioanalysis Group, Department d'Enginyeria Química, Universitat Rovira i Virgili, Avinguda Països Catalans 26, 43007 Tarragona, Spain.

E-mail: alex.fragoso@urv.cat

Abstract

Carbon nanomaterials can be prepared by several methods having in common that need a carbon source and often require high energies. In this study we report the synthesis and characterization of carbon nano-onions by annealing of commercially available nanodiamonds and explore for the first time their functionalization with a radio frequency Ar/O_2 plasma. Heat treatment of nanodiamonds at 1200ºC for 6 hours under argon atmosphere afforded small spherical carbon nano-onion particles of 3-4 nm diameter and 5-6 graphitic shells. The prepared CNOs were visualized by HRTEM and showed the characteristic XRD and Raman features. The results have been compared with a sample prepared by annealing at 1600ºC. Plasma functionalization in Ar/O_2 atmosphere was used to introduce oxygen moieties into the surface of synthesized CNOs. X-ray photoemission spectroscopy showed that oxygen-containing groups like C-O, C=O and O-C=O were introduced on the surface of CNOs, a process that is accompanied by a surface reorganization as evidenced by the change of I_D/I_G ratios in the Raman spectra, indicating a conversion of sp^2 to sp^3 as a result of functionalization in the surface of CNO.

Keywords: carbon nano-onion, nanodiamond, annealing, radio frequency plasma.

1. Introduction

Carbon nano-onions (CNOs) are multilayered fullerenes built from concentric graphitic shells forming quasi-spherical structures and can be considered as spherical analogues of multiwalled carbon nanotubes [1]. The first method to synthesize CNOs by intense electron beam irradiation of amorphous carbon as precursor was described by Ugarte in 1992, which also marks the discovery of this new nanocarbon form [2]. Following this report, many techniques were tried for efficient and gram-scale production of CNOs such as arc-discharge [3-5], chemical vapor deposition (CVD) [6,7] and radio frequency/microwave plasma [8]. These methods have some drawbacks related with the purity and quantity of the final product. For instance, arc-discharge often yields other carbon nanomaterials such as carbon nanotubes, the diameter of the CNOs is not homogenous and the purification methods are often destructive and affect the quality of the prepared CNOs. Recently, Stride proposed a method to prepare large CNOs by flash pyrolysis of naphthalene vapor followed by heating *in vacuo* to remove the unreacted precursor [9]

Kuznetsov [10] was the first to propose a precise way to produce homogenous and small CNOs of 5-8 carbon shells by vacuum annealing at high temperatures of ultra-dispersed nanodiamonds (NDs). This technique produces high yields of pure and small CNOs since it does not require any other catalyst and by adjusting the size distribution of the starting NDs before annealing it is possible to tune the size distribution of CNOs. Furthermore, this process could be scaled-up and may even be applied industrially. A detailed molecular dynamics simulation of the formation of NDs to CNOs was described by Tomita [11] who proposed that the heating treatment graphitize the NDs from the surface to the inner core until fully hollow CNOs are formed. However, the onset temperature of the start of graphitization of NDs until it is fully transformed to CNOs is

not clear and different values can be found in the literature which probably depends on the available devices for the annealing. Obraztsova et al. [12] observed that at around 1400 K (1127˚C) the first traces of graphitic layer started to appear with almost full transformation at 1800 K (1527˚C) but they have noticed reconfigured CNOs into a highly ordered hexagonal structure. On the other hand, Qiao et al. [13] synthesized CNOs by annealing NDs for 1 h at temperatures between 1100 and 1200˚C in an argon atmosphere. Their study revealed that CNOs begins to form at temperatures around 1100-1200˚C. Very recently, Mykhailiv et al. investigated the effect of synthesis conditions and a post-thermal treatment at lower temperatures on the structural and electrochemical properties of CNOs for supercarpacitor applications [14].

The applications of carbon nano-onions have been limited due to their intrinsically hydrophobic nature. To improve their solubility, several functionalization methods have been made either covalent [15-20] or non-covalent i.e. incorporated in composite materials [21-23] or using supramolecular interactions [24].

Plasma-based techniques are new and attractive ways to functionalize materials due to its simplicity and also because they are contaminant-free methods. No harsh chemicals were used, it is environmentally friendly and safe and easy to handle and operate. This method, which does not seem to tested in CNOs, induces less damage on the structure of the material, since the excited molecules produced during the plasma discharge attack the C=C bond creating open ends and defect sites as primary sites for functionalization. As in the case of multi-walled carbon nanotubes, the C=C bonds of CNOs are expected to be vulnerable to plasma activation with the formation of oxidized sites on the surface that can be the initial sites for further modifications [25].

In this work, we synthesized and prepared CNOs by annealing commercially available nanodiamonds at temperatures not exceeding 1200ºC under inert atmosphere.

The synthesized CNOs were further functionalized using a radio frequency (RF) plasma in Ar/O_2 atmosphere to introduce oxygenated groups on the surface of the CNOs [26]. This mild technique of functionalization would give newly transformed unique properties of CNO that can be used for other applications.

2. Experimental Section

Nanodiamonds (particle size: 2-8 nm) were obtained from TCI Europe BV and used as received. The annealing process was carried out on a quartz tubular furnace (HST 12/600, Carbolite, UK) able to heat up until 1200˚C. A sample of CNO prepared by annealing nanodiamonds at 1600ºC was used for comparison purposes [24].

2.1. Preparation

CNOs were prepared in two batches using different conditions. To prepare the first batch (CNO-1), 200 mg of nanodiamonds were loaded in a ceramic quartz boat and transferred to the furnace. The air in the furnace was removed by purging with nitrogen gas for several minutes. Annealing of nanodiamonds was performed at 1100˚C under nitrogen atmosphere with a heating ramp of 50˚C min^{-1}. The final temperature was kept for over a period of 3 h, and then the material was slowly cooled to room temperature.

The second batch (CNO-2) was prepared using 300 mg of nanodiamonds. The annealing was performed at 1200˚C under argon atmosphere at a heating ramp of 50˚C min^{-1}. The final temperature was maintained for 6 h and then the annealed sample was slowly cooled at room temperature. A portion of this sample was treated with 30% hydrogen peroxide for 3 h, washed and dried under vacuum at 50˚C (CNO-2*) [27].

2.2. Characterization

The annealed samples were characterized using High Resolution Transmission Electron Microscopy (HRTEM) on a Jeol 2011 instrument (from the Servei de Microscòpia of Universitat Autónoma de Barcelona) operated at 200 kV and adapted with diffraction patterns to visualize the structural form of the product before and after annealing. Samples were prepared in copper grids with a carbon layer and CNO samples were dispersed in ethanol.

Raman spectra were recorded in a RENISHAW inVia instrument equipped with a 514 nm excitation laser at 1 mW. A glass slide was used to hold the samples. The I_D/I_G ratio was calculated by dividing the areas of D-band and G-band peaks after background subtraction. X-ray diffraction (XRD) was performed using a Siemens D5000 diffractometer (Bragg-Brentano parafocusing geometry and vertical θ-θ goniometer) fitted with a curved graphite diffracted beam monochromator. The angular 2θ diffraction range was between 5˚ and 130˚. The data were collected with an angular step of 0.05˚ at 3 s per step and sample rotation. A low background Si (510) wafer was used as sample holder. $Cu_{k\alpha}$ radiation was obtained from a copper X-ray tube operated at 40 kV and 30 mA.

2.3. Radio Frequency (RF) Plasma Treatment

RF plasma treatment was carried out in a Diener Electronic GmbH Femto SRCE plasma instrument equipped with PC control. The low pressure plasma reactor consists of three main components: the vacuum chamber, the vacuum pump and a high frequency generator for plasma creation. A low pressure is created in the chamber by means of a vacuum pump at a pressure as low as 0.3 mbar and then mixture of Ar/O_2 is fed into the chamber continuously flowing to expel other contaminants for 2 min before the main

treatment. The working pressure was set at 0.4 mbar and when this pressure is achieved the generator is switched on and the process gas in the chamber is ionized. 40 mg of CNO-2 or CNO-2* were loaded in a Pyrex® glass container and mounted into the rotary drum of the plasma machine. The plasma system receives continuously fresh gas while contaminated gas is removed. Ar and O_2 concentration in the reaction were 75% and 25%, respectively. The plasma treatment was carried out for 5 min at a power of 30 W and 60 W and after this time, another 5 min was set to let the gas flush and vent the chamber.

The treated sample was removed and examined by X-Ray Photoemission Spectroscopy (XPS) (conducted at ICN2 facilities in Barcelona, Spain) and Raman spectroscopy. Ex-situ XPS experiments were performed at room temperature with a SPECS PHOIBOS 150 hemispherical analyzer at 10 eV pass energy using monochromatic Al Kα (1486.74 eV) radiation as excitation source in a base pressure of 10^{-10} mbar. Lorentzian deconvolution of the spectra was carried out using the Origin software (version 7).

3. Results and discussion

3.1. Preparation and characterization of CNOs by nanodiamond annealing

The structural transformation of ND to CNOs was first confirmed by direct visual observation as there was a significant change of color from gray to black of the starting NDs after annealing. The yield of CNO-1 and CNO-2 were (179 mg) 89.5% and (259 mg) 86.3%, respectively. These differences may be ascribed to the presence of water in the starting material.

The ND→CNO transformation was studied using HRTEM (Figure 1). The HRTEM images of the starting NDs showed the presence of the typical crystal lattice of diamond formed by parallel planes separated by ~0.19 nm, in good agreement with

literature reports [28] (Figure 1a). Inspection of HRTEM images of CNO-1 in Figure 1b showed particles not completely transformed into CNOs, in which graphitic shells of 2-3 layers are present around a ND core with a slightly increased interlayer distance of 0.21 nm. Therefore, these annealing conditions were not appropriate to transform completely the NDs in CNOS. In contrast, exposure of ND to the maximum temperature allowed by the furnace at 1200˚C for longer times (6 h) generated essentially spherical CNO particles of 3-4 nm diameter with no presence of ND lattices (Figure 1c). These particles were formed by an average of 5-6 graphitic shells with distances between the carbon layers around of 0.35 nm and indicate that these annealing conditions are adequate to form small diameter CNOs from NDs with no need of higher temperatures. In fact, a comparison with a sample annealed at 1600ºC [24,29] shows reconstructed hexagonal structures in the resulting CNOs due to the fusion of graphitic layers [30] due to the annealing at higher temperatures (Figure 1d).

Figure 1

XRD data was used to follow the transformation of NDs to CNOs (Figure 2). NDs have three characteristic peaks at 2θ values of 43º, 75º and 90º corresponding to the (111), (220) and (311) planes of sp^3-bonded diamond, respectively. On the other hand, the diffraction pattern of CNOs show two main peaks corresponding to sp^2 graphitic layers at 2θ values of 25º (002 plane) and around 43º (100 plane) [11]. Figure 2 shows the diffraction patterns obtained for the starting NDs and the products resulting from annealing (CNO-1 and CNO-2). In principle, the XRD signal can be generated from the coinciding scattering of many crystal planes and is thus proportional to the crystal volume of the whole sample. Therefore, in the case where large ND particles are not fully graphitized they would strongly contribute to the overall XRD signal and even small NDs that were fully transformed to sp^2 carbon will be overshadowed. This phenomenon was

clearly observed in CNO-1 in which the presence of peaks at 43º, 75º and 90º indicate that it contains the peaks of untransformed NDs and the appearance of a broad peak at 25º corresponding to the (002) plane of graphitic carbon is observed. In contrast, in CNO-2 the peaks at 75º and 90º are absent and only show the peaks at 25º and 43º (graphitic (100) plane), indicating a complete ND→CNO transformation in these conditions.

Figure 2

Raman spectroscopy is a very useful technique to characterize carbon structures that complements XRD and HRTEM, especially for the presence of the so-called D and G bands. The G band (~1580 cm^{-1}) is due to the sp^2 bonded carbons and indicates the presence of the graphitic layer. The D band (~1340 cm^{-1}) is related with defect modes and is very sensitive to any disruption between the configurations of the carbon material. The Raman spectrum of CNO-1 (Figure 3) shows two bands at 1340 and 1587 cm^{-1} with an I_D/I_G ratio of 1.07. These bands are broad and not well resolved, indicating an incomplete graphitization of the sample. Annealing at higher temperature for longer times as in CNO-2, gave a spectrum with well resolved peaks and $I_D/I_G = 0.94$, due to the stronger peak of the G-band (1584 cm^{-1}) which indicates that sp^3 carbons of the ND was converted to sp^2. The transformation of ND to CNO is also evident when comparing the Raman spectra of the CNO samples with that of ND. The latter shows a peak at 1329 cm^{-1} that corresponds to the sp_3 C-C bonds (close to bulk diamond which appears at 1332 cm^{-1}) and a second peak at 1596 cm^{-1} that is associated with adsorption of water molecules [31].

Figure 3

3.2. RF Plasma Functionalization of CNOs

The possibility to use an Ar/O_2 radio frequency plasma for functionalization of CNOs was then investigated. Since CNO-2 was the product that underwent a full graphitic

transformation, this sample was used for this study before and after treatment with hydrogen peroxide [27,29] to remove amorphous carbon (CNO-2*).

The chemical modification of the surface of CNOs arising from the plasma treatment was analyzed by XPS. XPS is a surface sensitive technique used to identify the functional groups attached to the surface of the material. Figure 4 shows the XPS survey spectra of CNO-2, CNO-2* and plasma treated samples together with the total percentages of carbon and oxygen. In all spectra, the distinctive existence of carbon and oxygen can be observed, even in pristine CNO-2. In this case, oxygen atoms come from air oxidation on the surface of CNO and humidity, which is about 10.80% (Figure 4a). There is a significant increase in the oxygen concentration after treatment with hydrogen peroxide, doubling the value of the percent of oxygen of pristine CNO (21.06%) indicating that this step can oxygenate the surface of CNOs (see below for further discussion) (Figure 4b). Treating the sample with plasma after purification removes unstable oxygen groups attached into the surface of purified CNOs. Since plasma can be used for both etching and functionalization, unbounded and unstable moieties are removed as indicated by the decrease in %O content in CNO-2-30W (Figure 4c) and CNO-2-60W (Figure 4d). On the other hand, the samples of pristine CNO-2 directly treated with plasma at 60W showed a minimal increase of oxygen content (about 1%), which clearly indicates that plasma treatment is a mild treatment to functionalize the CNO surfaces.

Figure 4

Further information on the nature of the functional groups on the CNO surface was obtained from the analysis of high-resolution XPS spectra (Table 1). Figure 5 shows the deconvolution of the C1s peak of each analyzed sample. The peak at 284.9 eV is attributed to the graphitic structure (C=C) and sp^2 carbons, while the peak centered at

286.2 eV is related with the sp^3-hybridized carbon atoms (C-C). The peaks at 287.7 eV and 289.4 eV correspond to the C-O and O-C=O functionalities, respectively. An additional weak peak at 291.5 eV, related to π-π^* transition levels associated with free electrons between the graphitic planes [26], can be seen in some of the samples. After the purification (Figure 5b), there was a decrease in sp^2 and sp^3 signals (49.65% and 33.87%) accompanied by an increase in C-O and O-C=O (14.6 % and 1.68%) as compared to CNO-2 (Figure 5a), indicating that purification introduced oxygen functionalities into the surface of CNO. Moreover, the π-π^* peak is only present in CNO-2 but not in CNO-2*, which indicates that the graphitic plane has been damaged decreasing the movement of free electrons. In plasma treated samples (Figures 5c and 5d), there is an increase of the sp^2 carbon signal, especially when treated at 30W, with a very slight restoration of the presence of π-π^* peak at 60 W. On the other hand, direct treatment of CNO-2* with plasma (Figure 5e) showed an obvious decrease in sp^2 carbons and an increase in all other peaks, which also indicates a successful oxygen functionalization in the surface of CNO.

Table 1. XPS analysis of CNO-2 samples before and after purification and plasma treatment at 30 and 60 W. The percents of each element were normalized to 100%.

	C 1s				***O 1s***		
Sample	sp^2	sp^3	C-O	O-C=O	H_2O	C-O	O-C=O
CNO-2	50.48	34.77	13.71	1.04	34.42	27.57	38.01
CNO-2*	49.65	33.87	14.80	1.68	13.90	46.24	39.86
CNO-2* 30W	55.43	33.06	10.94	0.57	17.47	46.95	35.58
CNO-2* 60W	49.92	35.01	13.77	1.30	13.25	36.54	50.21
CNO-2 60W	48.89	35.68	13.97	1.46	0.05	41.40	58.55

Figure 5

Analysis of the oxygen content of the samples was carried out based on the high resolution O1s spectra of the samples before and after treatment (Figure 6, Table 1). As can be seen, low RF power favors the formation of C-O functionalities, while increasing the power results in a much higher contents of carbonyl groups on the CNO surface, in agreement with the C 1s data. It is interesting to note the presence of water in all samples (except for CNO-2 treated at 60W), indicating a susceptibility to environment moisture, especially for CNO-2. This water contents decreases when the sample is purified and treated with plasma as well as when CNO-2 was directly treated with plasma. In the latter case, a hydrophobic surface seems to be generated thus moisture cannot affect the surface of CNO (Figure 6e, Table 1).

Figure 6

Raman spectroscopy was used to support the results in XPS for the change of sp^2 hybridized graphitic plane C=C to sp^3 carbon C-C before and after purification and plasma treatment as shown in Figure 7. The high sensitivity of the D and G Raman bands to the disorder in the surface of CNOs before and after purification and plasma treatment are shown in Figure 7. CNO-2 showed a lower I_D/I_G ratio of 0.94 due to the stronger intensity peak of the graphitic plane (sp^2) C=C at ~1584 cm^{-1} and lower disorder plane (sp^3) C-C at ~1337 cm^{-1}, which correlates well with the XPS findings. After purification, (CNO-2*) some of the sp^2 bonds seem to be converted to sp^3, thus there is a significant increase in the I_D/I_G ratio to 1.07. The sp^3 or D band has been enhanced due to the functionalization of the surface by purification as also reflected in XPS data. Interestingly, plasma treatment at 60W decreases the I_D/I_G ratio to 1.01, a result we attribute to an etching or removal of unstable disordered planes on the surface, which exposes the graphitic layer of CNOs as observed in the XPS spectra. These results allow us to propose

a mechanism similar to that represented in Figure 8 to account for the XPS and Raman results of the different treatments.

Figure 7

Figure 8

4. Conclusions

Heat treatment of ND at 1200ºC for 6 hours under argon atmosphere afforded small round CNO particles of 3-4 nm diameter and 5-6 graphitic shells. The CNO sample was characterized by HRTEM, XRD and Raman spectroscopy. Purification and plasma treated samples of CNOs generates oxygen functionalities into the surface as determined by XPS and Raman spectroscopy. This mild method opens the way to further covalent modifications of CNOs and studies are underway in this direction.

Acknowledgments

JPB thanks the Departament d'Enginyeria Química of Universitat Rovira i Virgili for a predoctoral scholarship. Financial support from Ministerio de Economía y Competitividad, Spain (Grant BIO2012-30936 to AF), is gratefully acknowledged.

References

1. a) Zeiger, M., Jäckel, N., Mochalin, V. N., and Presser V. (2016) Review: carbon onions for electrochemical energy storage. J. Mater. Chem A., 4: 3172-3196. b) Bartelmess, J., and Giordani, S. (2014) Carbon nano-onions (multi-layer fullerenes): chemistry and applications. Beilstein J. Nanotechnol., 5: 1980-1998. c) Plonska-Brzezinska, M. E., and Echegoyen, L. (2013) Carbon nano-onions for supercapacitor electrodes: recent developments and applications. J. Mater. Chem A., 1: 13703-13714. d) Kausar, A. (2017) Carbon nano onion as versatile contender in polymer compositing and advance application. Fuller. Nanotub. Car. N., 25: 109-123.
2. Ugarte, D. (1992) Curling and closure of graphitic networks under electron beam radiation. Nature, 359: 707-709.
3. Sano, N., Wang, H., Chhowalla, M., Alexandrou, I., and Amaratunga, G. A. J. (2001) Nanotechnology: synthesis of carbon "onions" in water. Nature, 414: 506-507.
4. Sano, N., Wang, H., Alexandrou, I., Chhowalla, M., Teo, K., and Amaratunga, G. A. J. (2002) Properties of carbon onions produced by an arc discharge in water. J. App. Phys., 92: 2783-2788.
5. Borgohain, R., Yang, J., Selegue, J. P., and Kim, D. Y. (2014) Controlled synthesis, efficient purification, and electrochemical characterization of arc-discharge carbon nano-onions. Carbon, 66: 272-284.
6. Wang, X., Xu, B., and Liu, X. (2006) Synthesis of Fe-included onion-like Fullerenes by chemical vapor deposition. Diam. Relat. Mater., 15: 147-150.
7. Yang, Y., Liu, X., Han, Y., Ren, W., and Yu, B. (2010) Ferromagnetic property and synthesis of onion-like fullerenes by chemical vapor deposition using Fe and Co catalysts supported on NaCl. J. Nanomater., 720937, 1-6.
8. Du, A., Liu, X., Fu, D., Han, P., and Xu, B. (2007) Onion-like fullerenes synthesis from coal. Fuel, 86: 294-298.
9. Choucaira, M., Stride, J. A. (2012) The gram-scale synthesis of carbon onions. Carbon, 50: 1109-1115.
10. Kuznetsov, V. L., Chuvilin, A. L., Butenko, Y. V., Mal'kov, I., and Titov. V. (1994) Onion-like carbon from ultra-disperse diamond. Chem. Phys. Lett., 222: 343-348.

11. a) Hawelek, L., Brodka, A., and Tomita, S. (2011) Transformation of nano-diamonds to carbon nano-onions studied by X-ray diffraction and molecular dynamics. Diam. Relat. Mater., 20: 1333-1339. b) Tomita, S., Burian, A., Dore, J. C., (2002) Diamond nanoparticles to carbon onions transformation: X-ray diffraction studies. Carbon, 40: 1469-1474.
12. Obraztsova, E. D., Fujii, M., Hayashi, S., Kuznetsov, V. L., Chuvilin, A. L., and Butenko, Y. V. (1998) Raman identification of onion-like carbon. Carbon, 36: 821-826.
13. Qiao, Z., Li, J., Zhao, N., Shi, C. and Nash P. (2006) Graphitization and microstructure transformation of nanodiamond to onion-like carbon. Scr. Mater., 54: 225-229.
14. Mykhailiv, O., Lapinski, A., Molina-Ontoria, A., Regulska, E., Echegoyen, L., Dubis, A. T., and Plonska-Brzezinska, M. E. (2015) Influence of the synthetic conditions on the structural and electrochemical properties of carbon nano-onions. ChemPhysChem, 16: 2182-2191.
15. Gao, Y., Zhou, Y. S., Qian, M., Hea, X., Redepenning, J., Goodman, P., Lic, H., Jiang, L., and Lu, Y. (2013) Chemical activation of carbon nano-onions for high-rate supercapacitor electrodes. Carbon, 51: 52-58.
16. Zhou, L., Gao, C., Zhu, D., Xu, W., Chen, F. F., Palkar, A., Echegoyen, L., and Kong, E. S. (2009) Facile functionalization of multilayer fullerenes (carbon nanoonions) by nitrene chemistry and "grafting from" strategy. Chem. Eur. J., 15: 1389-1396.
17. Rettenbacher, A. S., Elliot, B., Hudson, J. S., Amirkhanian, A., and Echegoyen L. (2006) Preparation and functionalization of multilayer fullerenes (carbon nano-onions). Chem. Eur. J., 12: 376-387.
18. Rettenbacher, A. S., Perpall, M. W., Echegoyen, L., Hudson, J., and Smith, D. W. (2007) Radical addition of a conjugated polymer to multilayer fullerenes (carbon nano-onions). Chem Mater., 19: 1411-1417.
19. Flavin, K., Chaur, M. N., Echegoyen, L., and Giordani, S. (2010) Functionalization of multilayer fullerenes (carbon nano-onions) using diazonium compounds and "click" chemistry. Org. Lett., 12: 840-843.
20. Molina-Ontoria, A., Chaur, M. N., Plonska-Brzezinska, M. E., and Echegoyen, L. (2013) Preparation and characterization of soluble carbon nano-onions by

covalent functionalization employing a Na-K alloy. Chem. Commun., 49: 2406-2408.

21. Breczko, J., Winkler, K., Plonska-Brzezinska, M. E., Vilalta, A., and Echegoyen, L. (2010) Electrochemical properties of composites containing small carbon nano-onions and solid polyelectrolytes. J. Mater. Chem., 20: 7761-7768.
22. Plonska-Brzezinska, M. E., Mazurczyk, J., Palys, B., Breczko, J., Lapinski, A., Dubis, A., and Echegoyen, L. (2012) Preparation and characterization of composites that contain small carbon nano-onions and conducting polyaniline. Chem. Eur. J., 18: 2600-2608.
23. Lapinski, A., Dubis, A. T., Plonska-Brzezinska, M. E., and Echegoyen, L. (2012) Vibrational spectroscopic study of carbon nano-onions coated with polyaniline. Phys. Stat. Sol. C., 9: 1210-1212.
24. Wajs, E., Molina-Ontoria, A., Nielsen, T. T., Echegoyen, L. and Fragoso, A,. (2015) Supramolecular solubilization of cyclodextrin-modified carbon nano-onions by host−guest interactions. Langmuir, 31: 535-541.
25. Chen, C., Liang, B., Ogino, A., Wang, X., and Nagatsu, M. (2009) Oxygen functionalization of multiwall carbon nanotubes by microwave-excited surface-wave plasma treatment. J. Phys. Chem., 113: 7659-7665.
26. Zhao, B., Zhang, L., Wang, X., and Yang, J. (2012). Surface functionalization of vertically-aligned carbon nanotube forests by radio-frequency Ar/O_2 plasma. Carbon. 50: 2710-2716.
27. Bystrzejewski, M., Rummeli, M. H., Gemming, T., Lange, H., and Huczko, A. (2010) Catalyst-free synthesis of onion-like carbon nanoparticles. New Carb Mater., 25: 1-8
28. Xiao, J., Ouyang, G., Liu, P., Wang, C., and Yang, G. (2014) Reversible nanodiamond-carbon onion phase transformations. Nano. Lett., 14: 3645-3652.
29. Bartolome, J. P., Echegoyen, L., and Fragoso, A. (2015) Reactive carbon nano-onion odified glassy carbon surfaces as DNA sensors for human papillomavirus oncogene detection with enhanced sensitivity. Anal Chem., 87: 6744-6751.
30. Tomita, S., Sakurai, T., Ohta, H., Fujii, M., and Hayashi, S. (2001) Structure and electronic properties of carbon nanoonions. J. Chem. Phys. 114: 7477-7482.
31. Mochalin, V. N., Shenderova, O., Ho, D., and Gogotsi, Y. (2012) The properties and applications of nanodiamonds. Nat. Nanotech. 7: 11-23.

Figure captions

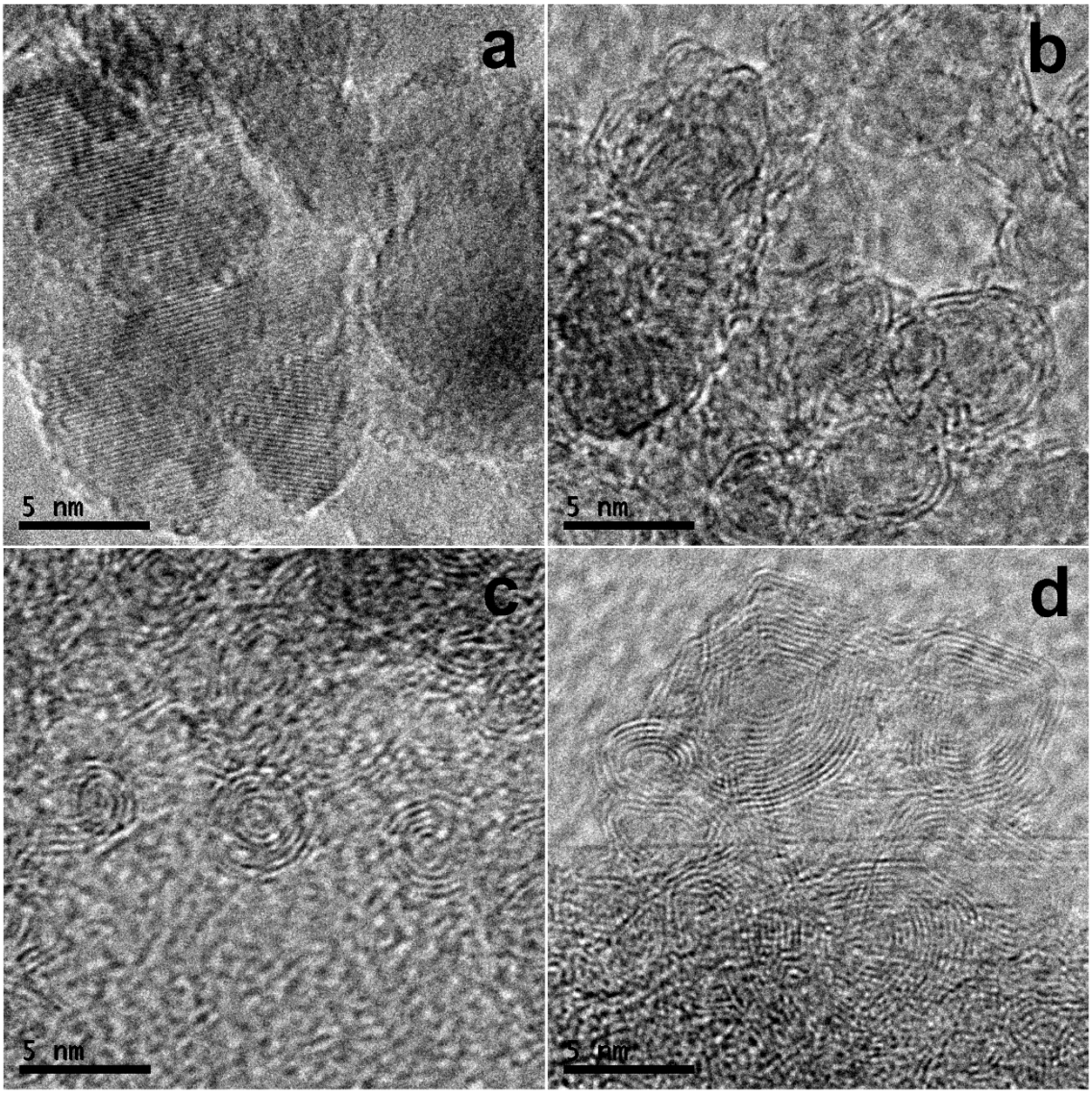

Figure 1. HRTEM images of a) ND, b) CNO-1, c) CNO-2 and d) ND annealed at 1600ºC.

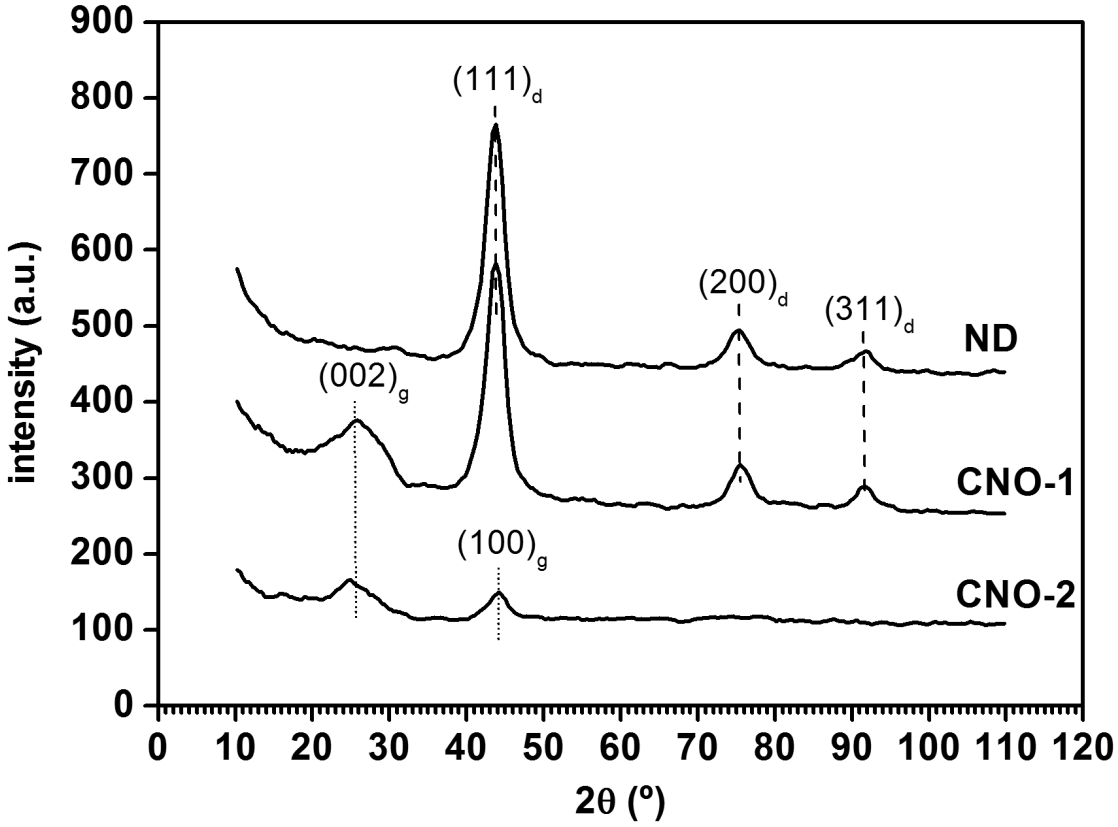

Figure 2. XRD patterns of ND, CNO-1 and CNO-2.

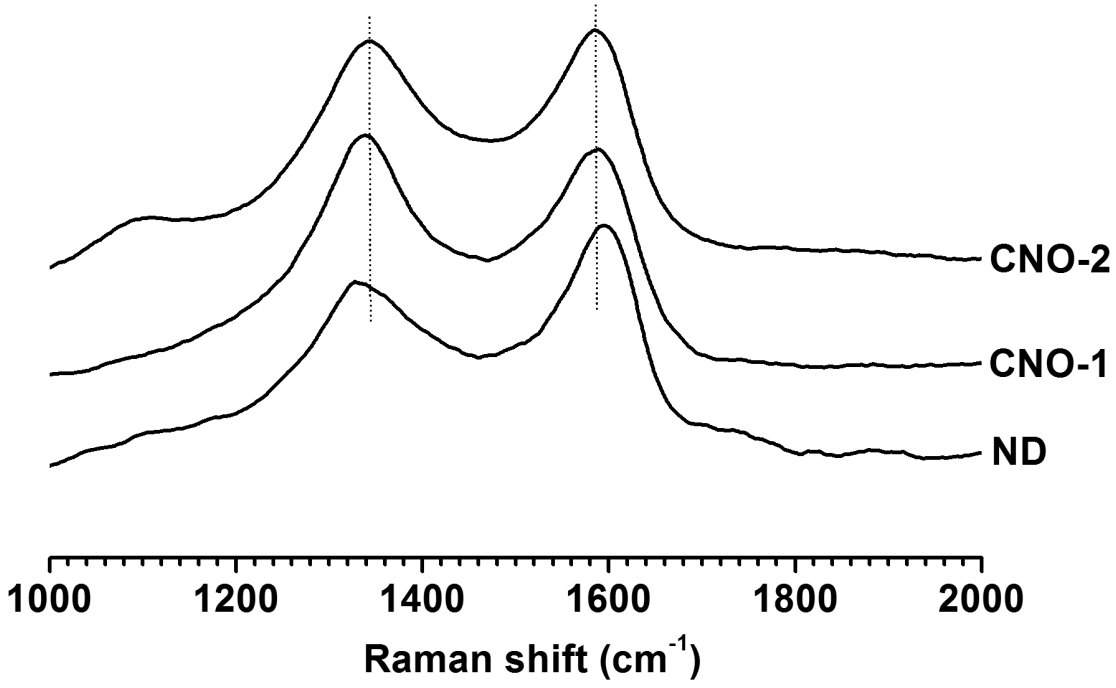

Figure 3. Raman spectra of ND, CNO-1 and CNO-2.

Sample	C (%)	O (%)
CNO-2 (a)	89.20	10.80
CNO-2* (b)	78.94	21.06
CNO-2* 30W (c)	83.13	16.87
CNO-2* 60W (d)	84.75	15.25
CNO-2 60W (e)	88.16	11.84

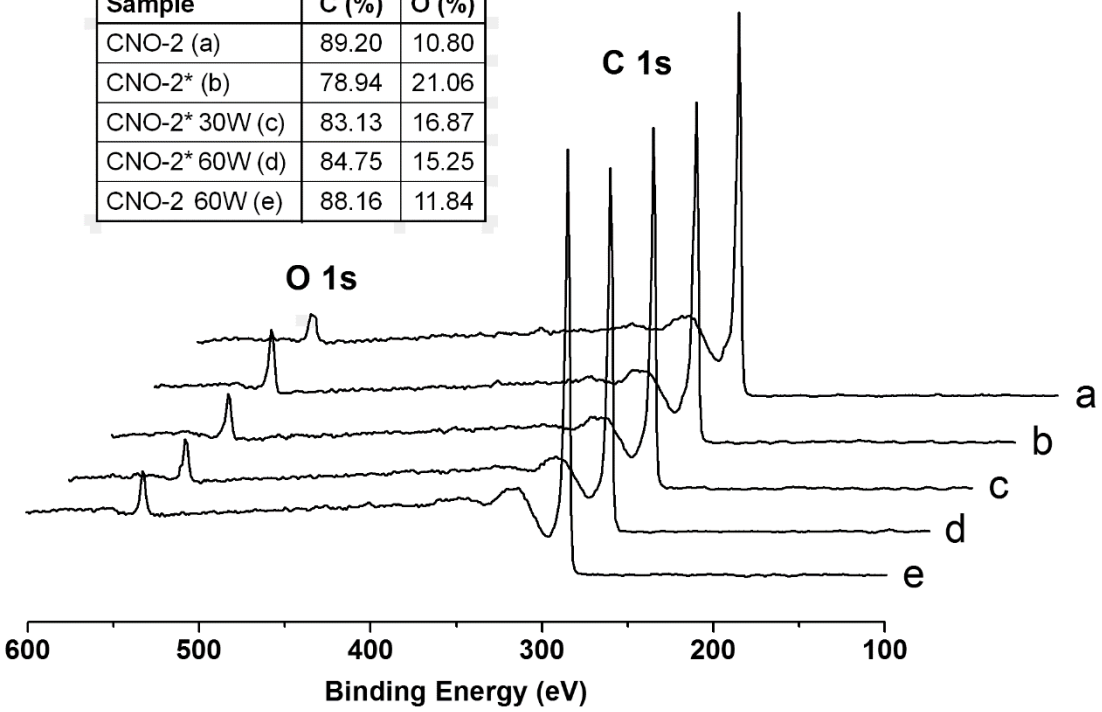

Figure 4. Survey XPS spectra of (a) CNO-2, (b) CNO-2*, (c) CNO-2* treated at 30W, (d) CNO-2* treated at 60 W and (e) CNO-2 treated at 60W.

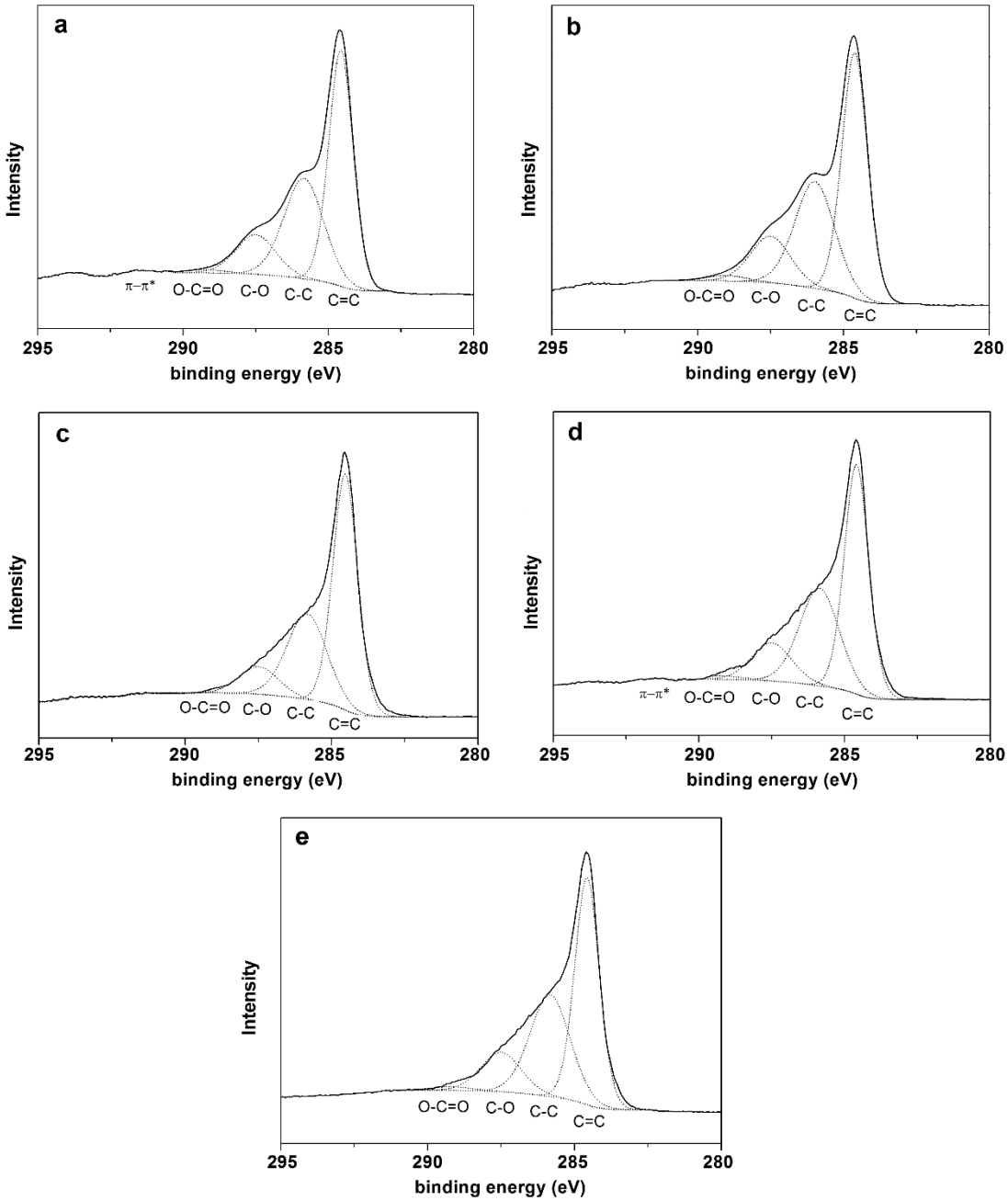

Figure 5. High resolution XPS C 1s spectra of (a) CNO-2, (b) CNO-2*, (c) CNO-2* treated at 30W, (d) CNO-2* treated at 60 W and (e) CNO-2 treated at 60W.

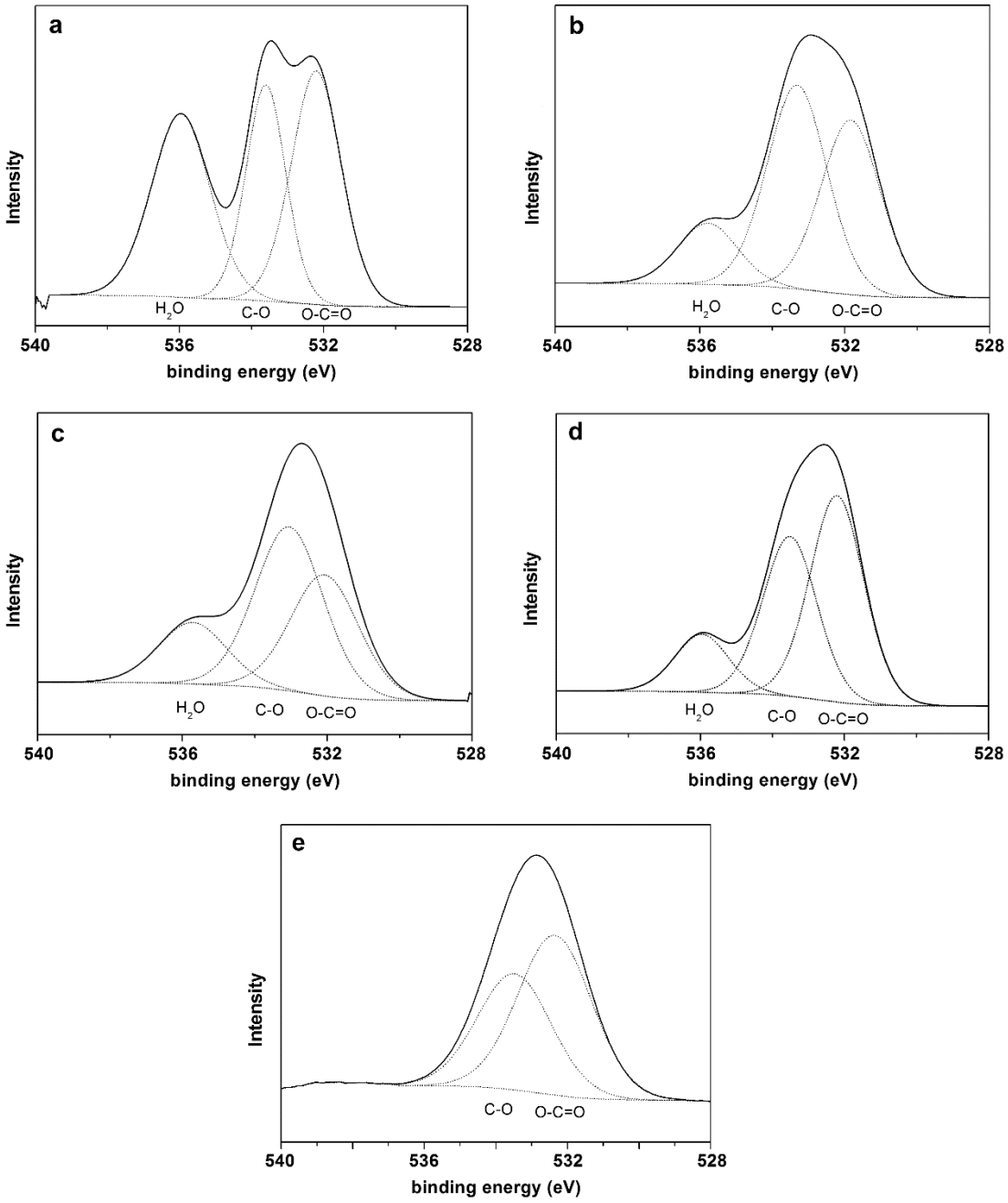

Figure 6. High resolution XPS O 1s spectra of (a) CNO-2, (b) CNO-2*, (c) CNO-2* treated at 30W, (d) CNO-2* treated at 60 W and (e) CNO-2 treated at 60W.

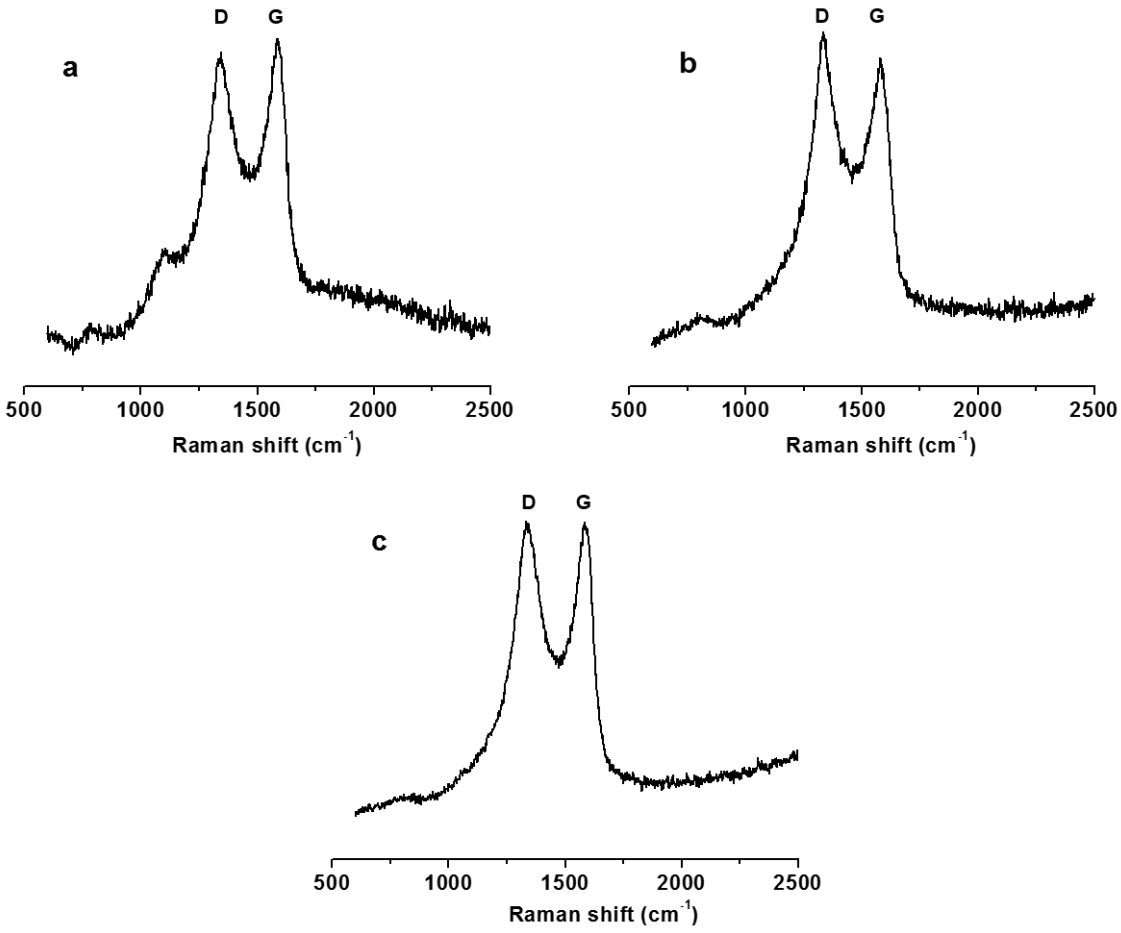

Figure 7. Raman spectra of a) CNO-2, (b) CNO-2*, (c) CNO-2* treated at 60 W.

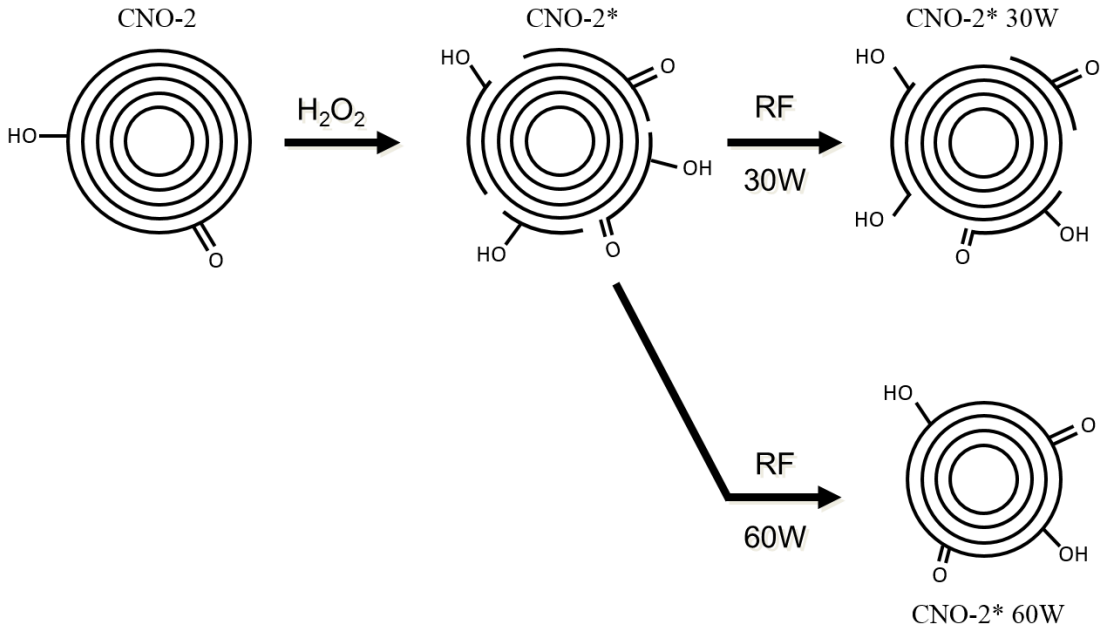

Figure 8. Proposed surface transformations of CNO-2 after purification and RF treatment.